ELSEVIER

International Journal of Mass Spectrometry 194 (2000) 121–132

International Journal of Mass Spectrometry

Collision-induced dissociation breakdown surfaces for *n*-alkylbenzene molecular ions in a quadrupole ion trap mass spectrometer

Cecilia Basic[1], Richard A. Yost*

Department of Chemistry, University of Florida, Gainesville, FL 32611-7200, USA

Received 12 March 1999; accepted 1 June 1999

Abstract

Complete collision-induced dissociation (CID) breakdown surfaces showing the $91^+/92^+$ ratios arising from the molecular ions (M^+) of *n*-butylbenzene, *n*-pentylbenzene, *n*-hexylbenzene, and *n*-octylbenzene have been obtained on a quadrupole ion trap mass spectrometer (QITMS). The $91^+/92^+$ ratios are plotted as a function of both resonant excitation time and voltage at a $q_z(M^+) = 0.300$ and at a constant He buffer gas pressure of 1.0×10^{-4} Torr (uncorrected ion gauge reading). Because the $91^+/92^+$ ratios reflect the average internal energy of the M^+ ions, the surfaces provide a complete map of the change in ion energy over a wide range of resonant excitation conditions. Comparisons of the $91^+/92^+$ ratios of the *n*-alkylbenzenes with those obtained using charge-exchange mass spectrometry (CEMS) indicate that the amount of internal energy deposited upon resonant excitation varies from ~1.5 eV for the M^+ ion of *n*-butylbenzene using 100 mV excitation, to ~7.5 eV for the M^+ ion of *n*-octylbenzene using 500 mV excitation. Moreover, calculations of the amount of internal energy deposited, as well as the percent energy transferred (%*E*), are found to increase as the size of the *n*-alkyl group of the M^+ ion is increased, paralleling the trend seen for the same M^+ ions following low-energy CID in a triple quadrupole mass spectrometer (TQMS) under single-collision conditions. This trend in the %*E* as a function of the size of the *n*-alkyl group parallels that found for the low-energy CID studies performed on a triple quadrupole mass spectrometer and thus indicates that the mechanism of CID in the QITMS is similar to that thought to occur in rf-only quadrupole collision cells. (Int J Mass Spectrom 194 (2000) 121–132) © 2000 Elsevier Science B.V.

Keywords: Collision-induced dissociation; *n*-alkylbenzenes; Breakdown surfaces; Quadrupole ion trap; Ion thermometers

1. Introduction

The amount of internal energy deposited into the ions upon resonant excitation in a quadrupole ion trap mass spectrometer (QITMS) has long been of interest [1–4]. Knowledge of the change in the average ion internal energy as a function of the amplitude and duration of the resonant excitation, or "tickle" potential, the amplitude of the rf trapping field (as reflected by the Mathieu parameter q_z of the precursor ion), or the pressure and nature of the buffer gas is critical to the complete understanding of the ion dissociation process and to the ability to compare tandem mass

* Corresponding author.

[1] Present address: Jet Propulsion Laboratory, California Institute of Technology, 4800 Oak Grove Drive, Pasadena, CA 91109.

Dedicated to Professor Jim Morrison on the occasion of his 75th birthday.

PII S1387-3806(99)00126-8

spectrometric (MS/MS) spectra obtained on a QITMS to those obtained using conventional beam mass spectrometers. Moreover, knowledge of the ion internal energies under a variety of conditions also helps determine the practical limits of the resonant excitation method for MS/MS analyses and in so doing defines the range of MS/MS fragmentation reactions possible using the QITMS.

Previous studies aimed at determining the average internal energy deposited into the ions in a QITMS upon resonant excitation have largely focussed on the use of the thermometer molecule *n*-butylbenzene [1–4]. The M^+ ion of *n*-butylbenzene (*m/z* 134) fragments via two principal pathways to form the $C_6H_5CH_3^+$ ion at *m/z* 92 and the $C_6H_5CH_2^+$ at *m/z* 91. Detailed studies of the relative rates of formation of the *m/z* 91 and 92 ions [5–7] reveal that the *m/z* 91 ion forms via direct cleavage of C_3H_7 with a high activation energy $\varepsilon_0 \approx 1.7$ eV, while the *m/z* 92 ion forms via a rearrangement and loss of C_3H_6 with a low $\varepsilon_0 \approx 1$ eV [7]. Photodissociation [6,8–10], charge-exchange (CEMS) [11], and photoelectron-photoion coincidence (PEPICO) studies [7] have revealed that the branching ratio of the *m/z* 91 and 92 ions, $91^+/92^+$, increases with increasing internal energy of the M^+ ion. A detailed comparison of the photodissociation and CEMS breakdown and the variety of internal energy effects encountered in studies of the $91^+/92^+$ ratio of the M^+ ion of *n*-butylbenzene has been presented by Boyd et al. [12].

Fragmentation of the molecular ion (M^+) of *n*-butylbenzene has been used extensively as a thermometer to measure the average internal energy deposited into an ion upon high-energy collision-induced dissociation (CID) [13], low-energy CID in a triple quadrupole mass spectrometer (TQMS) [14], and on both ion cyclotron resonance and hybrid magnetic sector/quadrupole (BQQ) mass spectrometers [15]. Louris et al. [1] used the fragmentation of the M^+ ion of *n*-butylbenzene to determine the internal energy deposited as function of the q_z value and the amplitude of the resonant excitation potential in a QITMS. In general, the ion internal energies were found to increase as the q_z value of the M^+ ion was increased and ranged from ~1 eV to 5 eV, over the q_z values (0.36 and 0.60) and voltages (2.7–14.4 $V_{p\text{-}p}$) employed. It was also noted that at the higher resonant excitation voltages, ejection of the M^+ ion competes with dissociation; thus, while the fragmentation efficiency increased, the overall CID efficiency decreased [1]. The distribution of ion internal energies in the QITMS was also estimated by measuring the fragment ion intensities arising from CID of the M^+ ion of tetraethylsilane, which fragments via the sequential loss of ethyl groups [16]. Since the activation energy ε_0 for each step is known, the internal energy distribution was estimated from the relative intensities of the fragment ions. The fragmentation patterns indicate that as the amplitude of the resonant excitation voltage is increased, the distribution of internal energies broadens, thus allowing access to higher energy the pathways, i.e., the loss of three C_2H_5 groups with an $\varepsilon_0 = 3.5$ eV [1].

Johnson et al. [2] have presented a more detailed study of the average internal energy transferred upon resonant excitation of the ions in a QITMS based on the $91^+/92^+$ ratio of the M^+ ion of *n*-butylbenzene. The effects of the resonant excitation frequency, amplitude, and time, as well as $q_z(M^+)$, and the nature and pressure of the buffer gas on the $91^+/92^+$ ratio were examined. These studies indicate that the $91^+/92^+$ ratio changes over the range of excitation voltages, $q_z(M^+)$, and buffer pressures employed. In general, the internal energy of the M^+ ion was found to increase as the $q_z(M^+)$ was increased, and to decrease as the He buffer pressure was increased. This latter observation is attributed to the increase in the number of cooling as opposed to activating collisions at the higher He pressure. The maximum $91^+/92^+$ ratio obtained over the range of experimental conditions employed was ~1.4, corresponding to an average internal energy of ~3.4 eV, assigned from the CEMS breakdown graph [11], in keeping with the energy range previously reported [1].

Liere et al. have also presented a study of the effects of resonant excitation frequency, amplitude, time, and $q_z(M^+)$ on the internal energy of the M^+ ion of *n*-butylbenzene, as well as the effect of the addition of a collisional cooling period prior to excitation [17]. The maximum $91^+/92^+$ ratio measured over the range

of excitation conditions employed without the addition of a cooling period was ~2.3, corresponding to an average internal energy of ~4.2 eV, assigned from the CEMS breakdown graph [11]. Upon addition of a 0–100 ms cooling period prior to excitation, it was found that the intensity of the *m/z* 91 and 92 ions first decreased from 10% to 0% and from 56% to 18%, respectively, as the cooling time was increased from 0 to 10 ms, while the intensity of the *m/z* 134 ion increased from 34% to 82% as the cooling time was increased from 0 to 15 ms. At cooling times >15 ms, the intensity of the *m/z* 91 ion remained at 0%, while that of the *m/z* 92 ion increased to 72% and that of the *m/z* 134 ion decreased to 30% [17]. A more detailed study into the effect of collisional cooling times revealed the occurrence of ion-molecule reactions between the *m/z* 91 and 92 ions and neutral *n*-butylbenzene in the trap, raising doubt as to whether the $91^+/92^+$ ratios are of value in assigning ion internal energies in the QITMS [18]. It was found that the *m/z* 91 ion reacts with *n*-butylbenzene to form $[M - H]^+$ (*m/z* 133) and $[M + CH]^+$ (*m/z* 147), while the *m/z* 92 ion undergoes charge-exchange with *n*-butylbenzene to form *m/z* 134 ions during the cooling times prior to excitation. The reaction rates varied as a function of the q_z of the reactant ions and the He buffer pressure. However, the measured rate constants are relatively low and similar in value over the range of conditions employed (e.g., $k = 3.1 \times 10^{-10}$ and 3.25×10^{-10} cm^3 molecule^{-1} s^{-1} for the *m/z* 91 and 92 ions, respectively, when $q_z(91^+) = 0.50$, $q_z(92^+) = 0.49$, and He pressure $= 9 \times 10^{-4}$ Torr), leading to the conclusion that these side reactions do not impair the estimation of ion internal energies from the measured $91^+/92^+$ ratios. The authors suggest that the somewhat higher rate constant for the *m/z* 92 ion may lead to a slight overestimation of the ion internal energies [18] and that the potential for ion-molecule reactions be recognized when investigating the effect of cooling times [19,20].

The $91^+/92^+$ fragment ion ratios of the M^+ ion of *n*-butylbenzene have also been employed in the development of an energy-resolved QITMS technique to estimate critical energies for dissociation [21], in the determination of the amount of internal energy deposited upon boundary activation [22,23], and in the characterization of photodissociation [24,25], surface-induced dissociation [26], and pulsed axial activation [27] in the QITMS. Other thermometer molecules have also been used to estimate the ion internal energies upon resonant excitation in the QITMS. Brodbelt et al. [28] have presented estimated ion internal energies upon resonant excitation based on the CID spectra of the M^+ ions of dimethyl phosphonate and dimethyl phosphite. The CID spectra reflect the isomerization of the phosphate ion to the phosphite tautomer which is strongly dependent on the collision conditions employed [29]. The activation energies for the various fragmentation pathways of the two isomers are also well known [30]. The authors suggest that the absence of the *m/z* 47 fragment ion ($\varepsilon_0 = 5.8$ eV) in the CID spectrum of the M^+ ion (*m/z* 110) of dimethyl phosphonate indicates that the average internal energy of the activated ions is <5.8 eV. Nourse et al. [31] report that a total of 29 eV of internal energy can be deposited into the M^+ ion of pyrene using six sequential stages of resonant excitation and mass-analysis (i.e., MS^6), each of which can deposit ~5 eV of energy. They also report that under "extreme" activation conditions ($6V_{0-p}$ resonant excitation voltage applied for 100 ms) fragment ions with estimated activation energies of 17 eV are formed from the M^+ ion of pyrene. Thus, while the majority of studies of the ion internal energies deposited upon resonant excitation in the QITMS indicate that the energies are in the low 2–4 eV range, substantially higher energies have also been reported.

In this paper we present the complete CID breakdown surfaces for the M^+ ions of *n*-butyl- (*m/z* 134), *n*-pentyl- (*m/z* 148), *n*-hexyl- (*m/z* 162), and *n*-octylbenzene (*m/z* 190), in which the $91^+/92^+$ ratios are plotted as a function of both the resonant excitation time and voltage. Average internal energies are then assigned to the M^+ ions using the $91^+/92^+$ ratios measured from the surface plateaus and the CEMS breakdown graphs reported for the respective *n*-alkylbenzene M^+ ions [32]. For simplicity, the studies were performed at a constant $q_z(M^+) = 0.300$ and at a constant He buffer pressure of 1.0×10^{-4} Torr (uncorrected ion gauge reading). The $q_z(M^+)$ and He

pressure, as well as any cooling times allowed between ion formation and the application of the excitation potential [17–19], dictate the initial internal energy of the M^+ ions prior to excitation. This initial energy then contributes to the total average internal energy following excitation as measured by the $91^+/92^+$ ratios. As with previous studies [1,2,17,21–23,26,27], the $91^+/92^+$ ratios provide single values which approximately represent an internal energy distribution for the specific M^+ ions of interest. In addition, differences in the kinetic shifts of the CEMS (dissociation rates $>10^3$ s^{-1}) versus the QITMS (dissociation rates $<10^3$ s^{-1}) experiments result in $91^+/92^+$ ratios that reflect different integration times. Despite these limitations, the $91^+/92^+$ ratios are of value in estimating ion internal energies following excitation in the QITMS and provide insight into the effects of changes in the resonant excitation time and voltage on the amount of energy deposited.

In an effort to gain insight into the efficiency of the kinetic-to-internal energy transfer process occurring in the QITMS, the assigned internal energies are then used to estimate the percent energy transferred (%E) upon CID in the QITMS, analogous to those calculated for the approach taken in the low-energy CID study of these M^+ ions performed under single-collision conditions in the rf-only collision cell of a TQMS [32]. In contrast to the TQMS studies, where a measure of the ion kinetic energy is readily available from the laboratory frame collision energies (E_{lab}) or the center-of-mass collision energies (E_{cm}), in this work an estimate of the amount of kinetic energy available for transfer in the QITMS was made by first calculating the Dehmelt pseudopotential well depth (D_z) and then calculating the average kinetic energy in both the r and z directions ($K.E._{avg,total}$) as follows [33]:

$$D_z = -\frac{eV^2}{4mz_0^2\Omega^2} \quad (1)$$

$$K.E._{avg,\ total} = \frac{8}{\pi^2} e\ D_z \quad (2)$$

Use of $K.E._{avg,total}$ in the calculation of the %E provides an estimate of the kinetic-to-internal energy transferred because $K.E._{avg,total}$ applies to collision-free conditions (leading to *higher* calculated $K.E._{avg,total}$ values than those likely when He buffer is present in the trap) and does not account for the added kinetic energy due to resonant excitation (leading to *lower* calculated $K.E._{avg,total}$ values than those likely upon excitation). However, trends in the calculated %E provide insight into the internal energy deposition process occurring in the QITMS. Topographical representations of the CID surfaces also provide quantitative insight into the relationship between resonant excitation time and voltage for the M^+ ions of interest.

2. Experimental

All experiments were performed on a Finnigan MAT (San Jose, CA) ion trap mass spectrometer (ITMS). High purity *n*-alkylbenzenes were purchased from Fluka Chemie AG, (CH-9470 Buchs, Switzerland) and used as received. Samples were introduced via Granville-Phillips (Boulder, CO) variable leak valves to a pressure of 2.0×10^{-6} Torr (uncorrected ion gauge reading) following three freeze-pump-thaw cycles. The He buffer gas was introduced to a pressure of 1.0×10^{-4} Torr (uncorrected) and the chamber was held at 100 °C. The M^+ ions of the *n*-alkylbenzenes were formed within the ion trap during a 1 ms electron ionization period, isolated at the upper apex of the stability diagram ($q_z = 0.15$, $q_z = 0.78$) using appropriate rf and dc voltages, and then resonantly excited at $q_z(M^+) = 0.300$. The resonant excitation frequency was optimized at each excitation voltage using a Forth program which varied the excitation frequency by varying the frequency delta value set in the ITMS software. A 1 ms period was added prior to varying the resonant excitation time to compensate for the finite rise time of the excitation voltage [2]. Other than this, no cooling times were used prior to excitation. The $91^+/92^+$ ratio surfaces were obtained by setting the resonant excitation voltage, varying the excitation time using the Forth programming option of the ITMS software, and then repeating this for each excitation voltage. All resonant excitation voltages are in V_{0-p}. The product ions were detected using the mass-selected instability scan with axial modulation.

2.1. Data manipulation

The ion intensities at each excitation voltage were extracted using Chrolist, a data reduction program developed in our laboratory [34] and normalized with respect to the sum of all the ions with relative intensities <5%. The CID surfaces of the $91^+/92^+$ ratios were constructed by calculating the $91^+/92^+$ ratios as a function of time for each of the excitation voltages and then forming a three-dimensional array. A five-point smoothing in both the *x* and *y* directions was performed on the array, which was then imported into a three-dimensional graphing program (Surfer, Golden Software, Inc., Golden, CO, USA). A 25 × 25 data grid was constructed using the inverse distance gridding method (weighting power = 2) and smoothed with a spline (*X* = *Y* expansion factor = 2).

The CID efficiencies were calculated as follows: fragmentation efficiency = $E_f = \Sigma F_i/(P + \Sigma F_i)$; collection efficiency = $E_c = (P + \Sigma F_i)/P_0$; and overall efficiency = $E_{\mathrm{CID}} = E_f E_c = \Sigma F_i/P_0$ where P_0 is the initial precursor ion intensity, and P and F_i are the precursor and fragment ion intensities following CID [35]. The Dehmelt pseudopotential well depth (D_z) and the average kinetic energy in both the *r* and *z* directions ($K.E._{\mathrm{avg,total}}$) were calculated using Eqs. 1 and 2 [33], respectively, for an ion trap with a stretched geometry; i.e., $z_0 = 0.7811$ [36]. The average internal energies of the *n*-alkylbenzene M^+ ions were assigned from the CEMS breakdown graphs [32] presented in Fig. 1. The percent energy conversions (%*E*) were then determined by dividing the average internal energies by $K.E._{\mathrm{avg,total}}$. Errors in the assigned ion energies were calculated as the range of internal energies arising from the range of observed $91^+/92^+$ ratios.

3. Results and Discussion

3.1. CID breakdown surfaces

The *m/z* 91 and 92 ions form the base peak in the CID mass spectra of the four *n*-alkylbenzenes M^+ ions of interest at resonant excitation times >1 ms at all the excitation voltages employed. The following

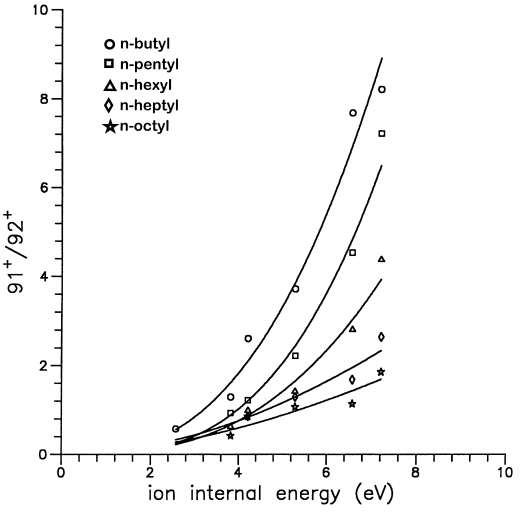

Fig. 1. The $91^+/92^+$ ratios as a function of the internal energy of the M^+ ions of the *n*-alkylbenzenes from charge-exchange mass spectrometry [32].

ions were also observed in the CID spectra obtained using a 300 mV excitation voltage and a 1.35 ms excitation time: *n*-butylbenzene *m/z* 135 (45%), 134 (15%), 119 (10%), and 105 (3%); *n*-pentylbenzene *m/z* 149 (26%), 148 (25%), 133 (45%), 119 (15%), 106 (15%), 105 (28%); *n*-hexylbenzene *m/z* 163 (19%), 162 (60%), 147 (8%), 133 (65%), 119 (12%), 105 (5%); *n*-octylbenzene *m/z* 191 (45%), 190 (32%), 175 (5%), 161 (12%), 148 (15%), 147 (20%), 134 (30%), 133 (55%), 119 (20%), and 105 (11%). At an excitation voltage of 500 mV and 0.9 ms excitation time, the *m/z* 91 and 92 ions are the base peak, but the relative intensities of all the other ions decrease to <20%.

Complete, three-dimensional CID breakdown surfaces showing the $91^+/92^+$ ratios arising from the M^+ ions of the four *n*-alkylbenzenes are presented in Fig. 2(a)–(d). Analogous surfaces would result had the intensity of either the *m/z* 91 and 92 fragment ions been plotted, while a complementary valley would result for plots of the intensities of the M^+ ions as a function of resonant excitation time and voltage. It can be seen that the *n*-butylbenzene and *n*-pentylbenzene $91^+/92^+$ ratios reach plateau values in both the *x* (resonant excitation voltage) and *y* (excitation time) directions. The $91^+/92^+$ ratios of the *n*-hexylbenzene

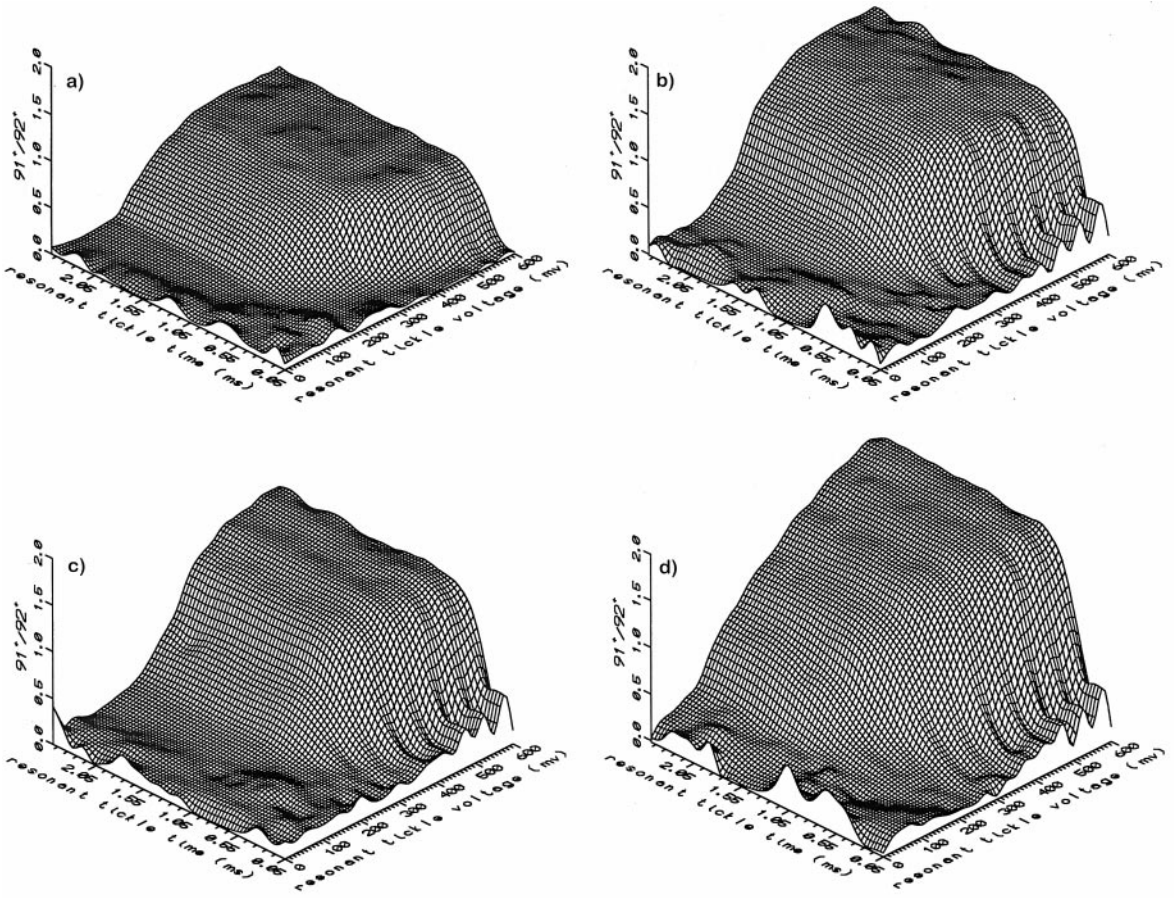

Fig. 2. Three-dimensional CID breakdown surfaces showing the $91^+/92^+$ ratios of (a) the M^+ ion of *n*-butylbenzene (*m/z* 134); (b) the M^+ ion of *n*-pentylbenzene (*m/z* 148): (c) the M^+ ion of *n*-hexylbenzene (*m/z* 162); and (d) the M^+ ion of *n*-octylbenzene (*m/z* 190).

and *n*-octylbenzene M^+ ion reach plateau values over the range of excitation times but not over the range of excitation voltages employed. Plateau values would presumably be reached if higher excitation voltages had been employed for these ions. Similar plateaus were observed in the two-dimensional plots of the $91^+/92^+$ ratios measured following low-energy CID of the M^+ ions of the *n*-alkylbenzenes obtained in the collision cell of a TQMS using E_{lab} between 15 and 85 eV with both Ar and N_2 collision gases (target gas thicknesses of 1×10^{14} molecules cm^{-2}, corresponding to single-collision conditions) [32].

The surfaces in Fig. 2(a)–(d) provide a complete map of the range of average internal energies which can be accessed for the M^+ ions of interest by varying either resonant excitation time or voltage at a $q_z(M^+) = 0.300$ and at a He buffer pressure of 1.0×10^{-4} Torr (uncorrected). They also indicate that there is an upper limit to the average internal energy which can be deposited into these M^+ ions upon resonant excitation; i.e., excitation for longer times at a given voltage does not necessarily result in increased energy deposition. This upper energy limit is due to the successful competition of collisional cooling with collisional activation. Similarly, excitation using higher voltages at a given resonant excitation time does not necessarily result in greater energy deposition; i.e., only that fraction of the M^+ ion population with sufficient internal energy will fragment by a given excitation voltage. The fact that a plateau

$91^+/92^+$ ratio value is reached, with a corresponding leveling of the M^+ ion intensity, indicates that a fraction of the ion populations always remains deep within the potential well and does not dissociate even at higher excitation voltages.

The upper average internal energy limits are seen more clearly in the topographical representations of the *n*-alkylbenzene surfaces presented in Fig. 3(a)–(h), in which each surface is shown on both linear (top) and log-log (bottom) scales. The $91^+/92^+$ ratio for the M^+ ion of *n*-butylbenzene varies from ~0.1 to a maximum plateau value of 0.7, corresponding to a range of assigned internal energies from 1.5 eV (extrapolated from the CEMS breakdown graph in Fig. 1) to an upper average internal energy of ~2.9 eV. The $91^+/92^+$ ratios of *n*-pentylbenzene range from 0.4 to 1.4, indicating a range of internal energies between ~3.0 and ~4.4 eV. The M^+ ion of *n*-hexylbenzene has a range of internal energies between ~3.2 and ~5.0 eV, while the internal energy of the M^+ ion of *n*-octylbenzene ranges from ~4.0 to ~7.5 eV (extrapolated from Fig. 1) over the range of excitation times and voltages employed. These results indicate that there is an increase in the amount of internal energy deposited as the size of the *n*-alkyl group increases, similar to that seen upon low-energy CID of these M^+ ions in the TQMS [32].

The topographical plots of the $91^+/92^+$ ratios in Fig. 3(a)–(h) illustrate the ability to "tune" the average internal energy deposited into the M^+ ions of the *n*-alkylbenzenes of interest upon resonant excitation by varying the excitation conditions. For example, at a resonant excitation voltage of 350 mV, the topographical plot of *n*-butylbenzene [Fig. 3(a)] indicates that 2.8 eV of internal energy ($91^+/92^+$ contour = 0.7) can be deposited in approximately 0.9 ms. Excitation times longer than this will not result in greater energy deposition at this voltage. The excitation conditions could be "softened" to reach 2.0 eV ($91^+/92^+$ contour = 0.2) by employing less time (350 mV for 0.5 ms) or less voltage (310 mV for 1 ms). Conditions of 400 mV for 0.5 ms could also be employed; however, as will be seen below, the CID efficiency drops at higher excitation voltages. The use of 350 mV and 0.9 ms in the resonant excitation would result in the deposition of 5.3 eV of energy ($91^+/92^+$ contour = 1.0) into the M^+ ion of *n*-octylbenzene. The specific excitation times and voltages, and the resulting assigned internal energies, are dictated by the unimolecular dissociation rates and the collisional excitation and collisional cooling rates of the particular M^+ ions of interest in this study. However, the topographical plots illustrate how similar internal energies can be achieved using different combinations of excitation times and voltages.

The hyperbolic shapes of the contour lines in Fig. 3(a)–(h) indicate that the relationship between resonant excitation time and voltage is not linear. Insight into the relationship between resonant excitation time and voltage can be better seen in the log-log topographical plots. Slopes of selected $91^+/92^+$ contour lines in the topographical log-log plots of the *n*-alkylbenzenes and the corresponding average internal energies assigned to these contour lines are presented in Table 1. An average slope of -1.4 ± 0.2 ms/mV is obtained over the internal energy range 2.6–4.4 eV for the M^+ ion of *n*-octylbenzene; the slope increases to -2.2 ms/mV at an average internal energy of 7.0 eV. The increase in slope indicates that longer resonant excitation times are required for higher internal energy deposition. The abrupt change in slope of the log-log topographical plots observed at lower resonant excitation voltages ($\lesssim$200 mV) may be attributed to the successful competition of collisional cooling of the ions with collisional activation. A similar break in the log-log plots of the resonant excitation voltage versus excitation time was found for the CID of the $(M + H)^+$ ion of diethyl ethylphosphonate [37].

3.2. CID breakdown graphs

Sample two-dimensional, time-resolved CID breakdown graphs showing the $91^+/92^+$ ratios for the M^+ ions of the *n*-alkylbenzenes using a 500 mV excitation voltage and the voltage-resolved graphs using a 1.5 ms excitation time are presented in Fig. 4(a) and (b), respectively. Note that the data in these graphs were not smoothed prior to plotting. In general, the plateau values of the $91^+/92^+$ ratios are found to increase as the size of the *n*-alkyl group

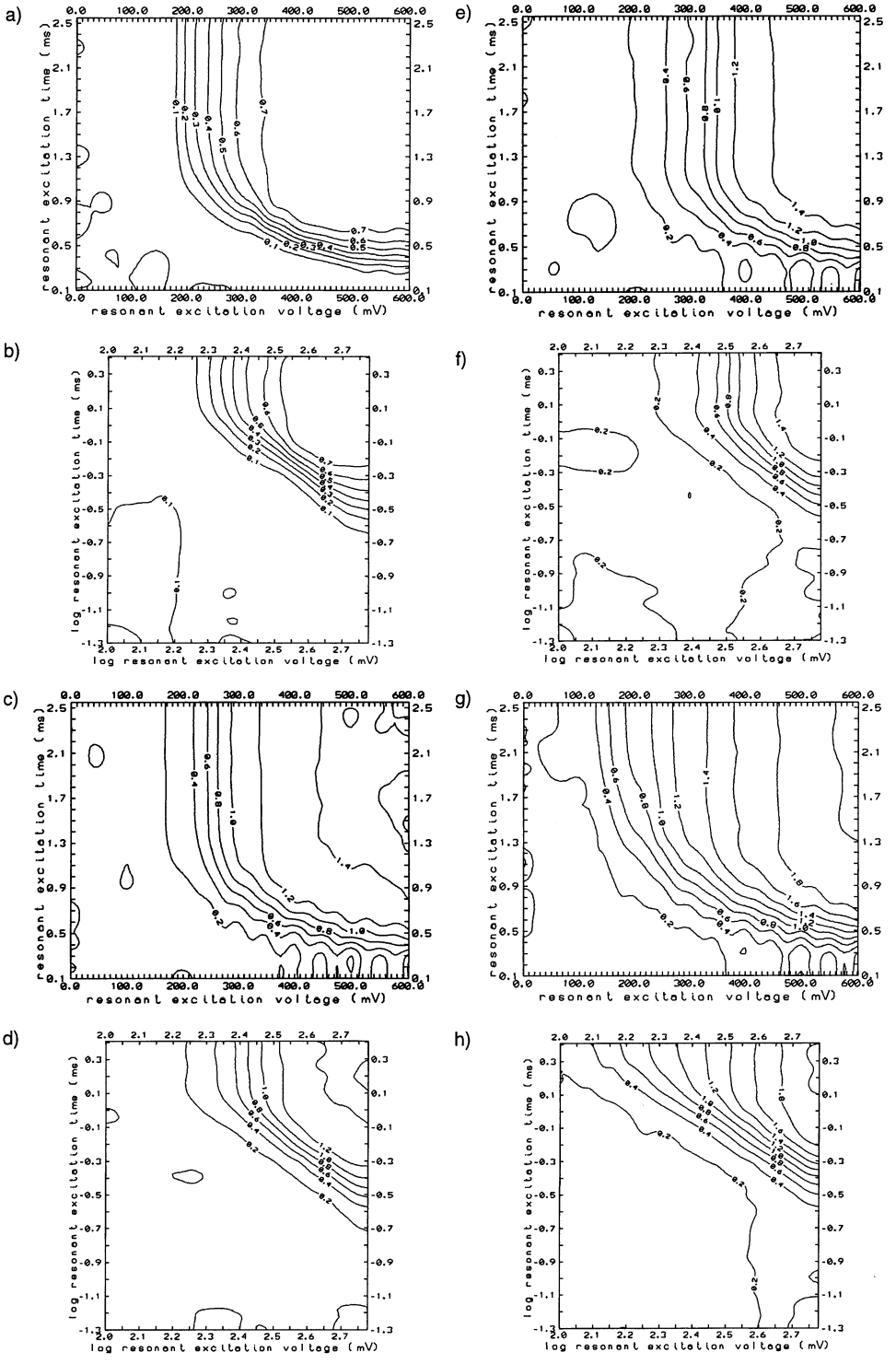

Fig. 3. Topographical plots of the CID breakdown surfaces in Fig. 2 on both linear and log-log scales. (a) and (b) *n*-butylbenzene; (c) and (d) *n*-pentylbenzene; (e) and (f) *n*-hexylbenzene; (g) and (h) *n*-octylbenzene.

Table 1
Slopes of the resonant excitation voltage versus excitation time in the log-log CID topographical plots at selected $91^+/92^+$ ratios for the M^+ ions of the *n*-alkylbenzenes

n-alkylbenzene	$91^+/92^+$ contour	Average internal energy (eV)[a]	Slope
butyl	0.6	2.6	−1.2
	0.7	2.7	−1.2
pentyl	0.6	3.4	−1.5
	1.2	4.0	−1.6
hexyl	0.6	3.7	−1.4
	1.0	4.4	−1.8
octyl	0.6	4.0	−1.4
	1.6	7.0	−2.2

[a] Average internal energies assigned from Fig. 1 [32].

increases, although *n*-pentyl- and *n*-hexylbenzene have approximately the same plateau values. This trend in $91^+/92^+$ values is the opposite of that observed in the TQMS study, where the $91^+/92^+$ plateau values in the CID breakdown graphs were found to decrease with increasing *n*-alkyl group size [32]. However, upon converting to E_{cm} values in the TQMS study and calculating the percent energy transfer (%*E*) using the assigned internal energies determined from the $91^+/92^+$ values at the onset of the plateaus (seen at an E_{lab} of 60 eV), the %*E* values were found to increase with increasing *n*-alkyl group size [32]. A similar increase in %*E* value with *n*-alkyl group size is also seen in the present QITMS studies (see below) and thus, in contrast to the TQMS studies, Fig. 4(a) and (b) directly reflect the trend in internal energy deposition as a function of *n*-alkyl group size. Differences in the $91^+/92^+$ ratio trends seen in the QITMS versus the TQMS studies [32] may be attributed to differences in the CID collision conditions; i.e., in the QITMS the M^+ ions not only undergo resonant excitation between collisions, but they also experience multiple collisions with He. In contrast, in the TQMS [32] the ions experienced single-collision conditions with N_2 or Ar and the M^+ ions do not experience continual excitation.

A summary of the fluences (V ms), CID efficiencies (E_f, E_c, and E_{CID}), and the assigned average internal energies determined from the time-resolved breakdown graphs using 300 mV (not shown) and 500 mV [Fig. 4(a)] resonant excitation voltages is presented in Table 2. The fluences, CID efficiencies, and internal energies were determined at the points on the two-dimensional breakdown graphs where the $91^+/92^+$ ratios begin to reach a plateau, similar to the approach taken in [32]. The time-resolved graphs were chosen since the voltage-resolved graphs were reconstructed from 30 time-resolved experiments acquired over a 60-min as opposed to a 2-min time period required for each of the time-resolved graphs. It can be seen from Table 2 that at a given resonant excitation voltage, an increase in the fluence is re-

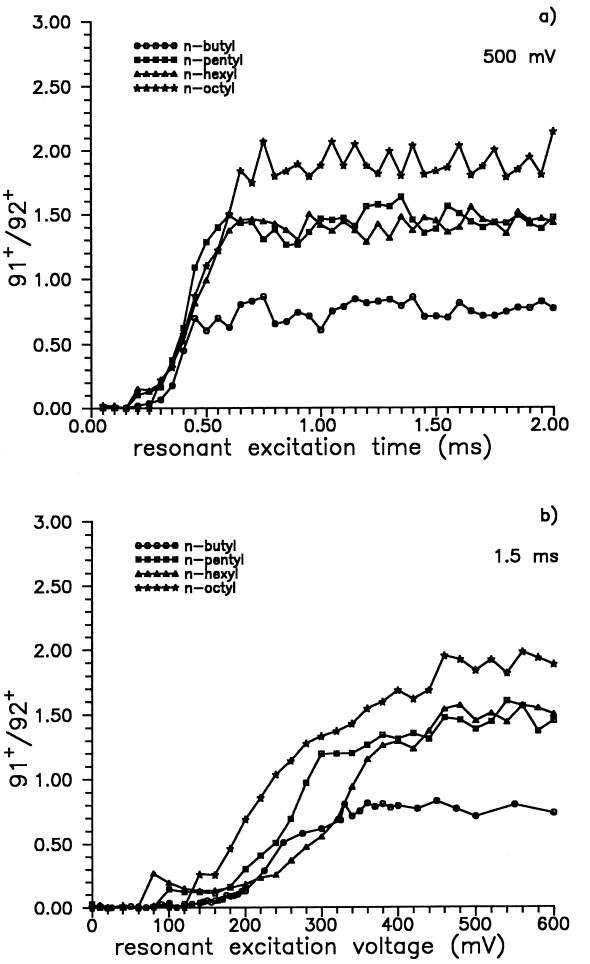

Fig. 4. The $91^+/92^+$ ratios from (a) time-resolved collision-induced dissociation of the M^+ ions of the *n*-alkylbenzenes, 500 mV excitation amplitude and (b) voltage-resolved CID of the M^+ ions, 1.5 ms excitation time.

Table 2
Fluences and CID efficiencies for the M^+ ions of the *n*-alkylbenzenes calculated at the onset of the $91^+/92^+$ plateaus for 300 and 500 mV excitation voltages

n-alkylbenzene[a]	Excitation voltage (V_{0-p})	$91^+/92^+$ plateau time (ms)	Fluence (V ms)	Normalized fluence	E_f[b] (%)	E_c[b] (%)	E_{CID}[b] (%)
butyl	0.300	1.05	0.315	0.78	94	54	51
pentyl	0.300	1.15	0.345	0.85	93	62	58
hexyl	0.300	1.20	0.365	0.90	85	75	64
octyl	0.300	1.35	0.405	1.0	94	64	60
butyl	0.500	0.55	0.275	0.61	96	26	25
pentyl	0.500	0.65	0.325	0.72	95	31	30
hexyl	0.500	0.75	0.375	0.83	96	30	29
octyl	0.500	0.90	0.450	1.0	96	41	40

[a] *n*-alkylbenzene pressures $\sim 2.0 \times 10^{-6}$ Torr (uncorrected ion gauge reading).
[b] E_f = fragmentation efficiency; E_c = collection efficiency; E_{CID} = CID efficiency.

quired to reach the $91^+/92^+$ plateau as the size of the *n*-alkyl group is increased; i.e., greater resonant power is required to reach the plateau values. It is interesting to note that the requisite fluence values remain approximately the same whether a 300 or 500 mV excitation potential is employed. However, the overall CID efficiency E_{CID} decreases at the higher excitation potential due to the decrease in collection efficiency E_c attributed to increased trapping losses [1,2]. The data in Table 2 thus indicate that while the fluence required to deposit a given amount of internal energy into the M^+ ions of the *n*-alkylbenzenes remains approximately constant, higher CID efficiencies can be obtained if the fluence is attained using longer resonant excitation times as opposed to higher excitation potentials.

Table 3 presents the $91^+/92^+$ ratios, the assigned average internal energies, and the corresponding percent energy transfer (%*E*) calculated from the time-resolved breakdown graphs using 300 mV (not shown) and 500 mV [Fig. 4(a)] excitation voltages. The assigned internal energies range from 2.7 eV for the M^+ ion of *n*-butylbenzene to 6.2 eV for the M^+ ion of *n*-octylbenzene using a 300 mV excitation voltage, and from 2.9 eV for the M^+ ion of *n*-butylbenzene to 7.5 eV for the M^+ ion of *n*-octylben-

Table 3
Internal energies and percent energy conversions from the *n*-alkylbenzene thermometers

n-alkylbenzene[a]	MW (u)	$91^+/92^+$	Internal energy[b] (eV)	D_z[c] (V)	$K.E._{avg,total}$[c] (eV)	%*E*[d]
			300 mV resonant excitation voltage			
butyl	134	0.65	2.7 ± 0.1	18.8	15.2	17.8
pentyl	148	1.15	4.12 ± 0.09	20.8	16.9	24.4
hexyl	162	0.59	3.66 ± 0.09	22.8	18.5	19.8
octyl	190	1.30	6.2 ± 0.3	26.7	21.6	28.7
			500 mV resonant excitation voltage			
butyl	134	0.75	2.9 ± 0.2	18.8	15.2	19.1
pentyl	148	1.43	4.4 ± 0.1	20.8	16.9	26.0
hexyl	162	1.45	5.0 ± 0.1	22.8	18.5	27.0
octyl	190	1.90	7.5 ± 0.4	26.7	21.6	34.7

[a] *n*-alkylbenzene pressures $\sim 2.0 \times 10^{-6}$ Torr (uncorrected ion gauge reading).
[b] Internal energies assigned from Fig. 1 [32]. Errors expressed as range of internal energies arising from the range of observed $91^+/92^+$ ratios.
[c] D_z and $K.E._{avg,total}$ values calculated with Eqs. (1) and (2) using V_{0-p} values for the drive rf potential at a $q_z(M^+) = 0.300$ and a stretched ion trap geometry.
[d] %*E* calculated from assigned internal energy divided by $K.E._{avg,total}$.

zene using a 500 mV excitation voltage, while the %E values are found to increase from ~18% for the M^+ ion of *n*-butylbenzene to ~29% using a 300 mV excitation voltage, and from ~19% to ~35% for the M^+ ion of *n*-octylbenzene using a 500 mV excitation voltage. The increase in internal energy deposition and in %E with increasing degrees of freedom of the M^+ ion is attributed to an increase in collisional activation cross-section, since an increase in ion mass from 134 to 190 leads to a small, and less favorable target gas-to-ion mass ratio. The increase in internal energy and in %E with increasing size of the *n*-alkyl group, or number of degrees of freedom of the M^+ ions, parallels the trends of percent energy transferred seen upon low-energy CID in the TQMS under single-collision conditions; i.e., in the TQMS, the average internal energy transferred was increased from 4.6 eV for the M^+ ion of *n*-butylbenzene using both N_2 and Ar collision gases, to 6.7 and 7.5 eV for the M^+ ion of *n*-octylbenzene using N_2 and Ar gases, respectively, with a corresponding increase in the %E from 45% to 87% with N_2 and from 33% to 72% with Ar [32]. Overall, the %E values for the QITMS are lower than those for the TQMS, suggesting that the efficiency of activation is not as high in the QITMS. However, the final average internal energies for the M^+ ions of the *n*-alkylbenzenes are approximately equal to those measured in the TQMS experiments, indicating that the continual, resonant excitation and multiple collision conditions operative in the QITMS lead to a similar amount of internal energy deposition as that experienced under single-collision conditions in the TQMS.

Use of the $K.E._{\mathrm{avg,total}}$ values in the calculation of the %E provides an estimate of the kinetic to internal energy transfer since $K.E._{\mathrm{avg,total}}$ applies only to collision-free conditions and does not account for the added kinetic energy due to resonant excitation. However, trends in %E provide insight into the mechanism of internal energy deposition in the QITMS. These trends in the %E as a function of the size of the *n*-alkyl group parallel those found in the TQMS study [32], indicating that the mechanism of CID in the QITMS is similar to that thought to occur in the quadrupole collision cell of a TQMS; i.e., the CID process likely occurs via the formation of a relatively long-lived M^+-N collision complex, (where N = the target gas species) in which the relative translational energy of the collision is converted into vibrational energy of the ion leading to the dissociation of the ion [32,38,39]. Based on this model, there should be a more efficient translational to vibrational energy transfer as the number of vibrational degrees of freedom of the M^+ ion increases. This is reflected in the effect of the *n*-alkyl group size on the average and %E transfer observed in both the low-energy TQMS and present QITMS studies.

4. Conclusions

Complete, three-dimensional, breakdown surfaces showing the $91^+/92^+$ ratios arising from CID of the M^+ ions of a series of *n*-alkylbenzenes provide a measure of the amount of internal energy deposited into the M^+ ions upon resonant excitation and provide insight into the mechanism of the CID process occurring in the QITMS. Plateau values of the $91^+/92^+$ ratios indicate that there is a limit to the amount of internal energy that can be deposited under a given set of resonant excitation conditions. These limiting values are attributed to the successful competition of cooling versus activating collisions with the He buffer gas as the resonant excitation times are increased. The average internal energy deposited upon resonant excitation at $q_z(M^+) = 0.300$ and at a He buffer pressure of 1.0×10^{-4} Torr (uncorrected) varies from ~1.5 eV for the M^+ ion of *n*-butylbenzene using 100 mV excitation to ~7.5 eV for the M^+ ion of *n*-octylbenzene using 500 mV excitation. This range of internal energies is in good agreement with those previously reported for the QITMS [1,2,17,28]. The amount of internal energy deposited and the percent energy transferred (%E) are found to increase as the size of the *n*-alkyl group of the M^+ ion is increased, reflecting an increase in excitation cross-section with increasing number of degrees of freedom of the ion. The trends in internal energy deposition and in %E parallel those seen for the same M^+ ions under single-collision conditions with N_2 and Ar in a

TQMS. However, while the final amounts of internal energy deposited into the M^+ ions of the *n*-alkylbenzenes are approximately equal in the QITMS and the TQMS studies, the %*E* values are lower for the QITMS, indicating that the efficiency of activation is not as high in the TQMS. This suggests that the CID process likely proceeds via a two-step activation/dissociation mechanism similar to that proposed for the low-energy CID process in a TQMS [32,38,39].

Acknowledgements

We would like to thank Nathan A. Yates for the Chrolist and Forth data acquisition software, Michael S. Freund for the data smoothing program, and John R. Eyler for many helpful discussions. The American Technology Initiative, funded in part by NASA, is gratefully acknowledged for partial funding of the work.

References

[1] J.N. Louris, R.G. Cooks, J.E.P. Syka, P.E. Kelley, G.C. Stafford, J.F.J. Todd, Anal. Chem. 59 (1987) 1677.
[2] J.V. Johnson, C. Basic, R.E. Pedder, B. Kleintop, R.A. Yost, in R.E. March, J.F.J. Todd (Eds.), Practical Aspects of Ion Trap Mass Spectrometry, Vol. 3, CRC, Boca Raton, FL, 1995, pp. 257–312.
[3] J. Gronowska, C. Paradisi, P. Traldi, U. Vettori, Rapid Commun Mass Spectrom. 4 (1990) 306.
[4] S.A. McLuckey, G.L. Glish, G.J. Van Berkel, Int. J. Mass Spectrom. Ion Processes 106 (1991) 213.
[5] P. Brown, Org. Mass Spectrom. 3 (1970) 1175.
[6] J.H. Chen, J.D. Hayes, R.C. Dunbar, J. Phys. Chem. 88 (1984) 4759.
[7] T. Baer, O. Dutuit, H. Mestdagh, C. Rolando, J. Phys. Chem. 92 (1988) 5674.
[8] S.T. Oh, J.C. Choe, M.S. Kim, J. Phys. Chem. 100 (1996) 13367.
[9] E.S. Mukhtar, I.W. Griffiths, F.M. Harris, J.H. Beynon, Int. J. Mass Spectrom. Ion Phys. 37 (1981) 159.
[10] I.W. Griffiths, E.S. Mukhtar, F.M. Harris, J.H. Beynon, Int. J. Mass Spectrom. Ion Phys. 43 (1982) 283.
[11] A.G. Harrison, M.S. Lin, Int. J. Mass Spectrom. Ion Phys. 51 (1983) 353.
[12] R.K. Boyd, F.M. Harris, J.H. Beynon, Int. J. Mass Spectrom. Ion Processes 66 (1985) 185.
[13] I.W. Griffiths, E.S. Mukhtar, R.E. March, F.M. Harris, J.H. Beynon, Int. J. Mass Spectrom. Ion Phys. 39 (1981) 125.
[14] P.H. Dawson, W.-F. Sun, Int. J. Mass Spectrom. Ion Phys. 44 (1982) 51.
[15] S.A. McLuckey, L. Sallans, R.B. Cody, R.C. Burnier, S. Verma, B.S. Freiser, R.G. Cooks, Int. J. Mass Spectrom. Ion Processes 44 (1982) 215.
[16] V.H. Wysocki, H.I. Kenttamaa, R.G. Cooks, Int. J. Mass Spectrom. Ion Processes 75 (1987) 181.
[17] P. Liere, R.E. March, T. Blasco, J.C. Tabet, Int. J. Mass Spectrom. Ion Processes 153 (1996) 101.
[18] P. Liere, V. Steiner, K.R. Jennings, R.E. March, J.C. Tabet, Int. J. Mass Spectrom. Ion Processes 167/168 (1997) 735.
[19] H.-F. Wu, J.S. Brodbelt, Int. J. Mass Spectrom. Ion Processes 115 (1992) 67.
[20] J.S. Brodbelt, in R.E. March, J.F.J. Todd (Eds.), Practical Aspects of Ion Trap Mass Spectrometry, Vol. 1, CRC, Boca Raton, FL, 1995, pp. 209–220.
[21] A. Colorado, J. Brodbelt, J. Am. Soc. Mass Spectrom. 7 (1996) 1116.
[22] C. Paradisi, J.F.J. Todd, U. Vettori, Org. Mass Spectrom. 27 (1992) 1210.
[23] C.S. Creaser, K.E. O'Neill, Org. Mass Spectrom. 28 (1993) 564.
[24] J.N. Louris, J.S. Brodbelt, R.G. Cooks, Int. J. Mass Spectrom. Ion Processes 75 (1987) 345.
[25] C.S. Creaser, M.R.S. McCoustra, K.E. O'Neill, Org. Mass Spectrom. 26 (1991) 335.
[26] S.A. Lammert, R.G. Cooks, J. Am. Soc. Mass Spectrom. 2 (1991) 487.
[27] S.A. Lammert, R.G. Cooks, Rap. Comm. Mass Spectrom. 6 (1992) 528.
[28] J.S. Brodbelt-Lustig, H.I. Kenttämaa, R.G. Cooks, Org. Mass Spectrom. 23 (1988) 6.
[29] H.I. Kenttämaa, R.G. Cooks, J. Am. Chem. Soc. 107 (1985) 1881.
[30] H.M. Rosenstock, K. Draxl, B.W. Steine, J.T. Herman, J. Phys. Chem. Ref. Data 6 (1977) (suppl 1).
[31] B.D. Nourse, K.A. Cox, K.L. Morand, R.G. Cooks, J. Am. Chem. Soc. 114 (1992) 2010.
[32] S. Nacson, A.G. Harrison, Int. J. Mass Spectrom. Ion Processes 63 (1985) 325.
[33] R.E. March, R.J. Hughes, Quadrupole Storage Mass Spectrometry and Its Applications, Wiley, New York, 1989.
[34] N.A. Yates, Ph.D. Dissertation, University of Florida, 1994.
[35] R.A. Yost, C.G. Enke, J. Am. Chem. Soc. 100 (1978) 2274.
[36] J.V. Johnson, R.E. Pedder, R.A. Yost, Rap. Comm. Mass Spectrom 6 (1992) 760.
[37] J.V. Johnson, R.A. Yost, P.E. Kelley, D.C. Bradrod, Anal. Chem. 62 (1990) 2162.
[38] D.J. Douglas, J. Phys. Chem. 86 (1982) 185.
[39] P.H. Dawson, D.J. Douglas, in F.W. McLafferty (Ed.), Tandem Mass Spectrometry, Wiley, New York, 1983, pp. 125–148.